Combined Quantum Chemical Density Functional Theory and Spectroscopic Raman and UV−vis−NIR Study of Oligothienoacenes with Five and Seven Rings

Reyes Malavé Osuna,[†] Xinnan Zhang,[‡] Adam Jay Matzger,[‡,§] Víctor Hernández,[†] and Juan Teodomiro López Navarrete*[,†]

Department of Physical Chemistry, University of Málaga, 29071-Málaga, Spain, and Department of Chemistry and the Macromolecular Science and Engineering Program, University of Michigan, 930 North University, Ann Arbor, Michigan 48109-1055

Received: February 3, 2006

In this article, we report the characterization of novel oligothienoacenes with five and seven fused thiophene rings, materials with potential applications in organic electronics. In contrast to usual α-linked oligothiophenes, these fused oligothiophenes have a larger band gap than most semiconductors currently used in the fabrication of organic field-effect transistors (OFETs) and therefore they are expected to be more stable in air. The synthesis of these fused-ring oligomers was motivated by the notion that a more rigid and planar structure should reduce defects (such as torsion about single bonds between α-linked units or S-syn defects) and thus improve conjugation for better charge-carrier mobility. The conjugational properties of these two molecular materials have been investigated by means of FT-Raman spectroscopy, revealing that conjugation still increases in passing from the five-ring oligomer to that with seven-rings. DFT and TDDFT quantum chemical calculations have been performed, at the B3LYP/6-31G** level, to assess information regarding the minimum-energy molecular structure, topologies, and absolute energies of the frontier molecular orbitals (MOs.) around the gap, vibrational normal modes related to the main Raman features, and vertical one-electron excitations giving rise to the main optical absorptions.

I. Introduction

Oligothiophenes (multiple thiophene rings joined by single bonds) are a leading class of organic semiconductors materials for new technologies.[1] In particular, α-sexithiophene and its derivatives have been employed as the active layer in organic electronic devices.[2] However, deviation from planarity may decrease conjugation in α-oligothiophenes through torsion about single bonds or S-syn defects. Chemists have been interested in making fused-ring analogues with the idea that a more rigid structure will reduce defects and thus improve conjugation for better charge-carrier mobility. The synthesis of molecules consisting of as many as five fused rings (pentathienoacene) has previously been reported.[3] However, the synthetic route is inefficient and not applicable to longer thienoacenes because of the extremely poor solubility of the longer oligomers.

Some of us have recently reported on an improved synthetic methodology designed to efficiently prepare thienoacenes.[4] This new route has allowed production of pentathienoacene in large scale and with improved yield, and also the extension of the series to heptathienoacene (seven fused rings), through the coupling of two brominated thienothiophenes (two fused rings) or two dithienothiophenes (three fused rings), respectively, via a sulfide bridge, followed by a ring-closing reaction at the sulfide bridge to form the central fused ring. These oligothienoacenes have more efficient molecular packing than usual oligothiophenes because they adopt face-to-face (π-stacked) packing motifs in contrast to the packing arrangement commonly found in α-linked oligothiophenes (face-to-edge or herringbone packing). Furthermore, oligothienoacenes have a larger band gap than most semiconducting materials used in organic field-effect transistors (OFETs) and therefore are expected to have improved environmental stability.

Molecular spectroscopy is a fundamental tool to establish structure−property relationships guiding the design of new and improved molecular materials. In particular, Raman spectroscopy is very well suited for the study of conjugated systems. Raman frequencies and intensities are experimental observables emerging directly from the π-conjugated frame which account for the most important electronic signatures of oligothiophenes. The Effective Conjugation Coordinate (ECC) model[5] predicts two main trends for the Raman spectral profiles of π-conjugated molecules: (a) selective enhancement of particular scatterings associated with collective C=C/C−C stretching vibrations of the π-conjugated backbone (this phenomenon relates to the occurrence in these types of one-dimensional systems of an electron−phonon mechanism which is at the origin of their outstanding optical and electrical features) and (b) frequency downshift of these enhanced Raman bands upon relaxation of the molecular structure as the consequence of either greater π-electron conjugation in the neutral state or quinoidization induced by ionization. When these experimental spectroscopic data are combined with reliable quantum chemical calculations, it is possible to assess precisely the relevant molecular parameters which would be very difficult to evaluate by other conventional experimental techniques. First principles quantum chemical calculations in the framework of DFT theory are very well suited to model extended π-conjugated systems due to implemented electron-correlation effects.

* To whom correspondence should be addressed. E-mail: teodomiro@uma.es.
[†] University of Málaga.
[‡] University of Michigan.
[§] E-mail: matzger@umich.edu.

10.1021/jp0607263 CCC: $33.50
Published on Web 03/25/2006

In this contribution, we use Raman spectroscopy to analyze the conjugational properties of oligothienoacenes with five and seven rings and investigate their optical properties by means of UV−vis−NIR absorption spectroscopy. The whole set of experimental data has been interpreted with the help of DFT and TDDFT quantum chemical calculations, at the B3LYP/6-31G** level, regarding the minimum-energy molecular structure, topologies, and absolute energies of the frontier molecular orbitals (MOs) around the gap, vibrational normal modes associated to the most outstanding Raman scatterings, and one-electron vertical excitations involved in the main optical absorptions.

II. Experimental and Theoretical Details

Pentathienoacene (**5TA**) and heptathienoacene (**7TA**) were prepared according to the previously reported procedure.[4] Both compounds were purified by sublimation ($7.0-8.0 \times 10^{-5}$ Torr, 150−160 °C for **5TA** and $4.0-5.0 \times 10^{-5}$ Torr, 230−245 °C for **7TA**). UV−vis absorption spectra of pentathienoacene and heptathienoacene were recorded with a CARY 300 Bio UV−vis spectrophotometer in tetrahydrofuran (THF) solution ($<10^{-6}$ M) at room temperature. THF was purified by passage through a column packed with activated alumina. Emission spectra were collected on a FluoroMax-2 spectrometer in CH_2Cl_2 solution ($<10^{-8}$ M). The fluorescence spectral profiles were found to be independent of the excitation wavelength in the region between 330 and 370 nm for pentathienoacene and 350−390 nm for heptathienoacene.

Fourier transform infrared absorption (FTIR) spectra were recorded on a Bruker Equinox 55 spectrometer. Compounds were ground to a powder and pressed in KBr pellets. FTIR spectra, with a spectral resolution of 2 cm^{-1}, were collected by averaging 50 scans. Interference from atmospheric water vapor was minimized by purging the instrument with dry argon before starting the data collection. FT-Raman scattering spectra were collected on a Bruker FRA106/S apparatus and a Nd:YAG laser source ($\lambda_{exc} = 1064$ nm), in a backscattering configuration. The operating power for the exciting laser radiation was kept to 100 mW in all the experiments. Samples were analyzed as pure solids in sealed capillaries. Typically, 1000 scans with 2 cm^{-1} spectral resolution were averaged to optimize the signal-to-noise ratio.

Density functional theory (DFT) calculations were carried out by means of the Gaussian 03 program[6] running on a SGI Origin 2000 supercomputer. Becke's three-parameter exchange functional combined with the LYP correlation functional (B3LYP)[7] was employed because it has been shown that the B3LYP functional yields similar geometries for medium-sized molecules as MP2 calculations do with the same basis sets.[8,9] Moreover, the DFT force fields calculated using the B3LYP functional yield IR spectra in very good agreement with experiments.[10,11] The standard 6-31G** basis set was used to obtain optimized geometries on isolated entities.[12] C_{2v} symmetry constraints were imposed during the geometry optimization of each system (namely, all geometrical parameters of half the molecule were allowed to vary independently except for the planarity of fused rings). On the resulting ground-state optimized geometries, harmonic vibrational frequencies and IR and Raman intensities were calculated with the B3LYP functional.

We used the often-practiced adjustment of the theoretical force fields in which calculated harmonic vibrational frequencies are uniformly scaled down by a factor of 0.96 for the 6-31G** calculations, as recommended by Scott and Radom.[10] This scaling procedure is often accurate enough to disentangle serious experimental misassignments. All quoted vibrational frequencies reported in the paper are thus scaled values. The theoretical spectra were obtaining by convoluting the scaled frequencies with Gaussian functions (10 cm^{-1} width at the half-height). The relative heights of the Gaussians were determined from the theoretical Raman scattering activities.

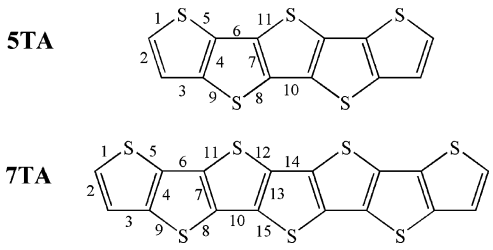

Figure 1. Chemical structures of the two oligothienoacenes and their corresponding abbreviation to be used throughout the text (atom numbering is to be used for Table 2).

Vertical electronic excitation energies were computed by using the time-dependent DFT (TDDFT) approach.[13,14] The 20 lowest-energy electronic excited states were computed for all the molecules. The computational cost of TDDFT is roughly comparable to that of single-excitation theories based on an HF ground state, such as single-excitation configuration interactions (CISs). Numerical applications reported so far indicate that TDDFT formalism employing current exchange-correlation functionals performs significantly better than HF-based single-excitation theories for the low-lying valence excited states of both closed-shell and open-shell molecules.[15,16] TDDFT calculations were carried out using the B3LYP functional and the 6-31G** basis set on the previously optimized molecular geometries obtained at the same level of calculation. Molecular orbital contours were plotted using Molekel 4.3.[17]

III. Results and Discussion

A. UV−vis Absorption Data. Chemical structures of the two oligothienoacenes analyzed in this article are depicted in Figure 1, whereas Figure 2 displays their normalized electromagnetic absorption and emission spectra. Both **5TA** and **7TA** show a strong electromagnetic absorption in the visible, together with a weaker band at higher energy. Well-resolved vibronic structures, due to the planar and rigid structure of the compounds, are evident in both absorption spectra (the precise wavelength values corresponding to the various vibronic peaks of each optical absorption are provided in Table 1). The two optical absorptions red shift upon increasing the number of fused rings, with a commensurate intensity increase for the longest wavelength band upon passing from the five-ring to the seven-ring thienoacene. In comparison to its nonfused α-linked oligothienyl counterpart, α-terthiophene (**3T**), it was observed that **5TA** shows a quite similar absorption maximum (354 and 355 nm, respectively), despite the different number of sulfur linkages: an indication that the six double bonds in each dictate this property.[18] The same trend was found for the longer oligothienoacene; **7TA** displays a longest λ_{max} of absorption (396 nm), rather close to that of nonfused α-quaterthiophene (**4T**, 390 nm), which also contains eight double bonds. In addition, the electromagnetic absorption envelope is found to be significantly narrower for the fused oligothienoacenes than for their nonfused oligothienyl counterparts with the same number of double bonds; furthermore, the vibronic transitions are much more clearly distinguishable for the former set of compounds, consistent with absorption from a single molecular conformation in solution. However, contrary to the similar absorption maxima

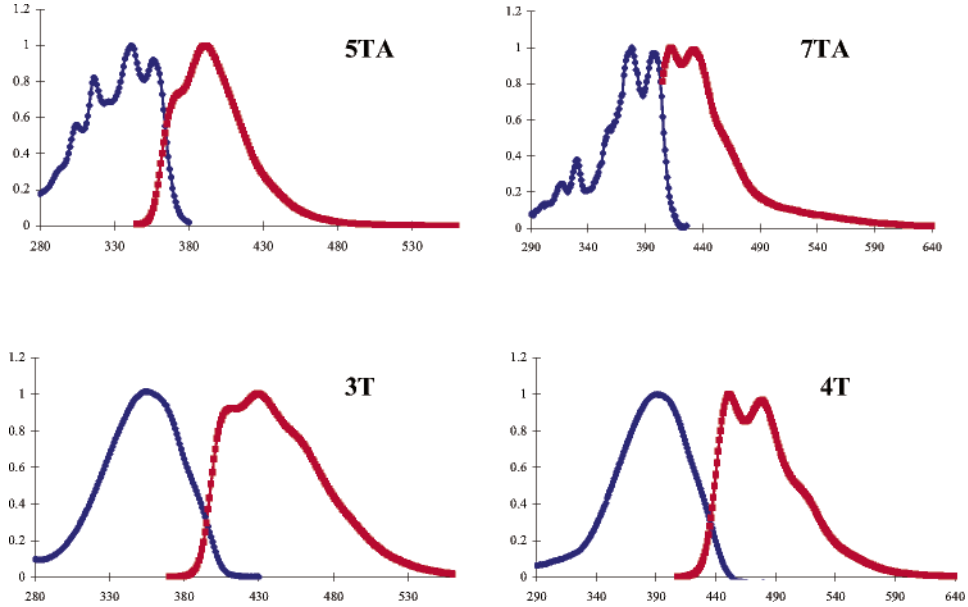

Figure 2. Normalized UV−vis absorption (blue) and fluorecence emission (red) spectra of **5TA**, **7TA**, **3T**, and **4T** in THF.

TABLE 1: UV−vis Absorption Maxima (λ_{max}) of 5TA and 7TA in THF

compound	λ_{max} in nm
5TA	355, 340, 324; 315, 303, 292
7TA	396, 375, 356; 327, 314, 301

TABLE 2: Optimized B3LYP/6-31G Values (in angstroms) for Selected Skeletal Bond Lengths of 5TA and 7TA**

bond number	5TA	7TA	bond number	5TA	7TA
1	1.751	1.751	9	1.760	1.760
2	1.367	1.367	10	1.419	1.418
3	1.423	1.423	11	1.756	1.756
4	1.394	1.394	12		1.756
5	1.742	1.741	13		1.396
6	1.420	1.419	14		1.417
7	1.395	1.395	15		1.756
8	1.756	1.756			

of **5TA** and **7TA** to those of **3T** and **4T**, respectively, the fluorescence emissions of the two former compounds are significantly blue shifted with respect to those measured for the two latter ones. Consequently, the Stokes shift is smaller for the oligothienoacenes, consistent with a closer geometric match between the ground state and the first singlet excited state for these two systems.

B. Optimized Geometries and Theoretical Electronic Transitions. To gain a deeper insight into the chain-length dependence of the molecular structure in these oligothienoacenes, geometry optimizations were performed within the framework of the DFT, for **5TA** and **7TA** using B3LYP/6-31G** model chemistry (Table 2 summarizes the optimized distances for selected skeletal bonds of **5TA** and **7TA**). The optimized geometries reveal that the various thienyl units of a given fused oligomer display similar C_α═C_β and C_β−C_β bond lengths (i.e., of around 1.396 and 1.419 Å, respectively) except for the outermost C_α═C_β bonds at each side end of the oligothienoacene, which are the shortest C═C bond lengths of the whole π-conjugated path (i.e., 1.367 Å). Although this result can be related to the fact that this is the only double bond of the π-conjugated path experiencing no ring fusion and the accompanying strain, a similar trend of variation is usually predicted for the C_α═C_β bond lengths in nonfused α-oligothiophenes. This effect has been attributed to less efficient π-conjugation from the middle of the oligomer chain toward its ends. The DFT//B3LYP/6-31G** calculations predict nearly the same geometry for the corresponding fused rings from one oligomer to another, and consequently, the geometric parameters are expected to quickly reach saturation upon chain lengthening (i.e., this theoretical result can be related to the presence of many electron-rich sulfur atoms surrounding a highly polarizable π-conjugated frame of alternating C═C/C−C bonds). The mean single−double CC bond-length-alternation (BLA) parameter, related to the difference between the average lengths of single and double π-conjugated CC bonds, steadily decreases from 0.043 to 0.021 Å in going from the end rings toward the central one in **7TA**.

TABLE 3: TDDFT//B3LYP/6-31G Vertical One-Electron Excitations (values are given in nanometers) Related to the Strongest UV−vis Absorptions of 5TA and 7TA**

compound	experimental[a]	TDDFT//B3LYP/6-31G**	description
5TA	355 (340, 324)	349 (f = 0.754)	H → L
	315 (303, 292)	306 (f = 0.104)	H − 1 → L
7TA	396 (375, 356)	397 (f = 1.202)	H → L
	327 (314, 301)	323 (f = 0.097)	H − 1 → L

[a] Values in parentheses correspond to vibronic peaks.

To provide insight into the nature of the UV−vis absorptions observed experimentally for the chromophores, the lowest-energy electronic excited states of **5TA** and **7TA** were calculated at the B3LYP/6-31G** level using the TDDFT approach on their previously optimized ground-state molecular geometries. Transition energies and oscillator strengths are listed in Table 3 along with the description of the experimental absorptions in terms of the dominant one-electron vertical excitations. Figure 3 sketches a comparative diagram with the B3LYP/6-31G** energies of the frontier molecular orbitals around the gap for **5TA** and **7TA** and for the two nonfused oligothienyl model systems (all-syn **3T** and **4T**), whereas Figure 4 shows the topologies of selected MOs of the four compounds, as a guide to the TDDFT analysis of the optical absorptions of the fused oligothienoacenes.

Theoretical calculations predict the appearance of two strong electronic transitions in the visible region (see Table 3). The absorption bands, measured in THF solution, at 355 nm (**5TA**)

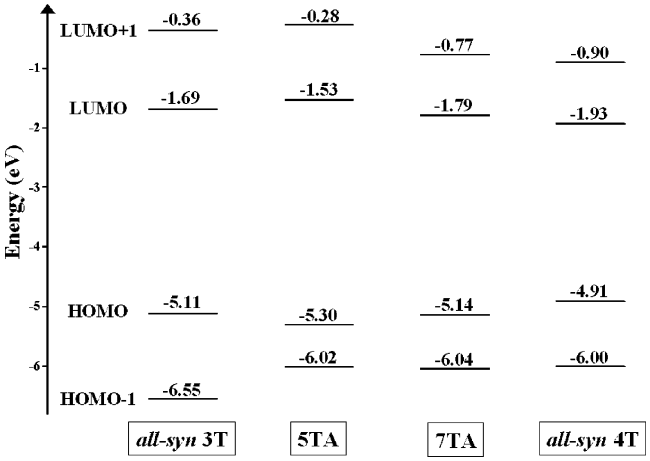

Figure 3. Comparison between the B3LYP/6-31G** energy levels around the band gap region for **5TA** and **7TA** and two linear α-oligothienyl model counterparts with the same number of double bonds (all-syn **3T** and **4T**).

and 396 nm (**7TA**) correspond to the excitation to the first singlet excited state, which is computed at 349 nm for **5TA** (with an oscillator strength, *f*, of 0.754) and at 397 nm for **7TA** ($f = 1.202$). This vertical transition is mainly described by a one-electron excitation from the highest occupied molecular orbital (HOMO) to the lowest unoccupied molecular orbital (LUMO). Thus, TDDFT model chemistry reproduces, with very good accuracy, the experimental wavelengths for the optical transitions of the two fused oligothienoacenes under study and nicely accounts also for the red shift of the $\pi-\pi^*$ transition in passing from the shorter system to the longer one.

Both the HOMO and LUMO of the oligothienoacenes are of π-nature and spread over the whole frame of fused rings (see Figure 4). As for the HOMO, the C═C bonds are π-bonding and have an alternating phase with respect to their adjacent C═C bonds, whereas for the LUMO, the C═C bonds are π-antibonding and the $C_\beta-C_\beta'$ and $C_\alpha-C_\alpha'$ are bonding reminiscent of a quinoidal form. As can be seen in Figure 4, the topologies of these two frontier MOs in the oligothienoacenes are almost identical to those of the nonfused α-oligothiophenes. Furthermore, from the comparison between the B3LYP/6-31G** energy levels around the band gap region for **5TA** and the all-syn **3T** model system sketched in Figure 3, it can be concluded that the introduction of two sulfur linkages between the inner β-positions of the α-terthienyl compound leads to a stabilization of the HOMO by 0.192 eV and a destabilization of the LUMO by 0.156 eV, so that the overall effect is an increase in the energy gap from 3.416 eV in all-syn **3T** to 3.766 eV in **5TA**. As for **7TA** and the all-syn **4T**, their comparative study reveals that the bridging of the various inner β-positions of the latter system by three sulfur linkages downshifts the HOMO by 0.229 eV and upshifts the LUMO by 0.136 eV, thus enlarging the HOMO−LUMO gap from 2.979 eV in the all-syn **4T** to 3.344 eV in **7TA**.

The electromagnetic absorptions experimentally measured at 315 nm (**5TA**) and 327 nm (**7TA**) must be correlated to the TDDFT//B3LYP/6-31G** transitions computed for **5TA** at 306 ($f = 0.104$) and for **7TA** at 323 nm ($f = 0.097$). In both cases,

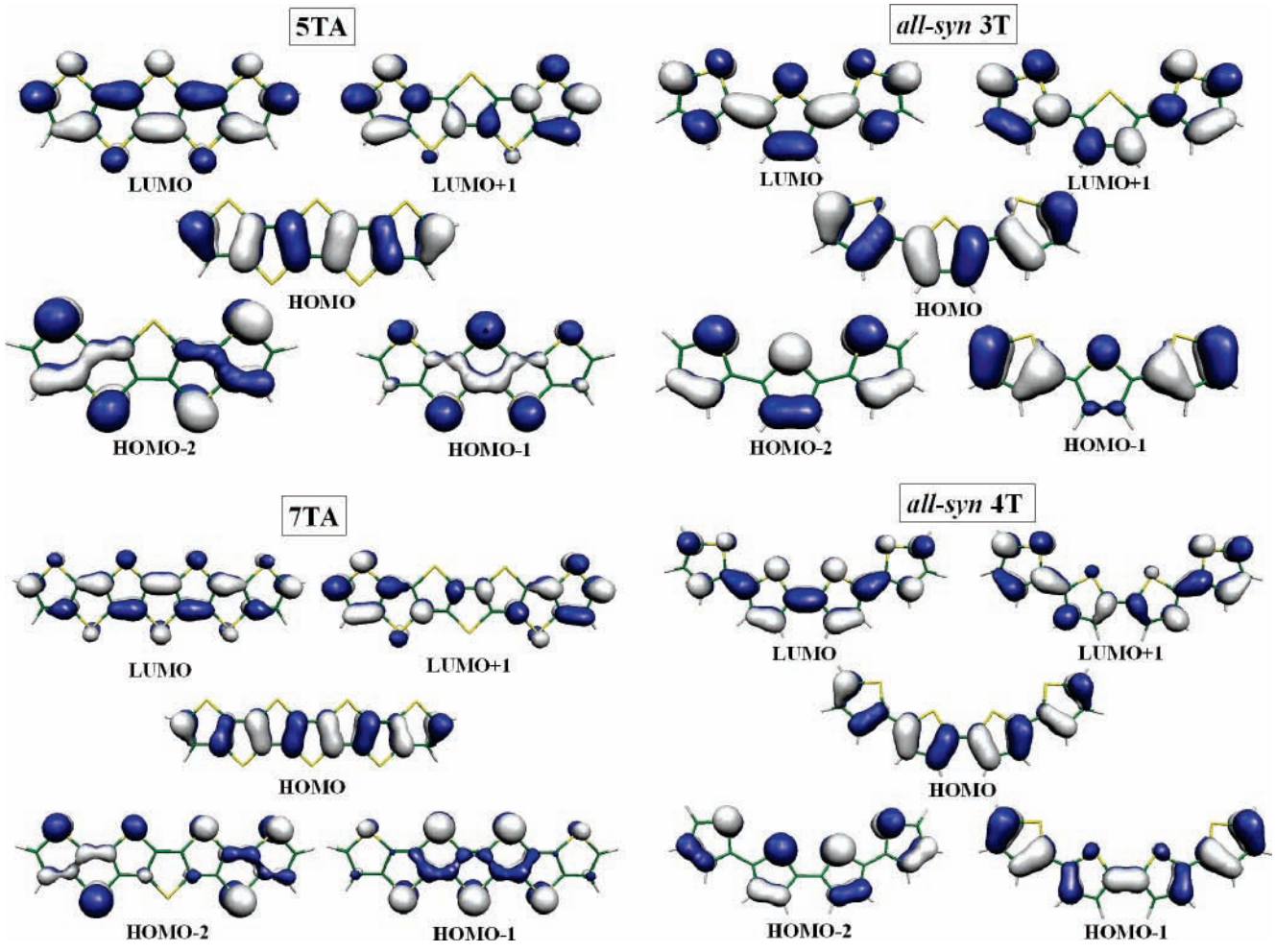

Figure 4. DFT//B3LYP/6-31G** electronic density contours (0.03 e/bohr^3) for selected MOs of **5TA**, **7TA**, all-syn **3T**, and all-syn **4T**.

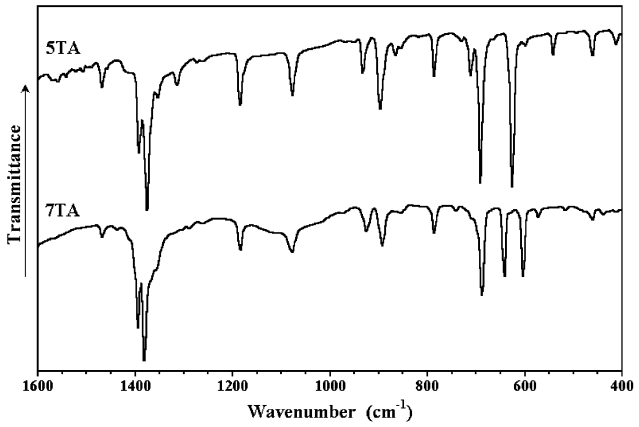

Figure 5. FTIR spectra of **5TA** and **7TA** in the 1600−400 cm^{-1} range.

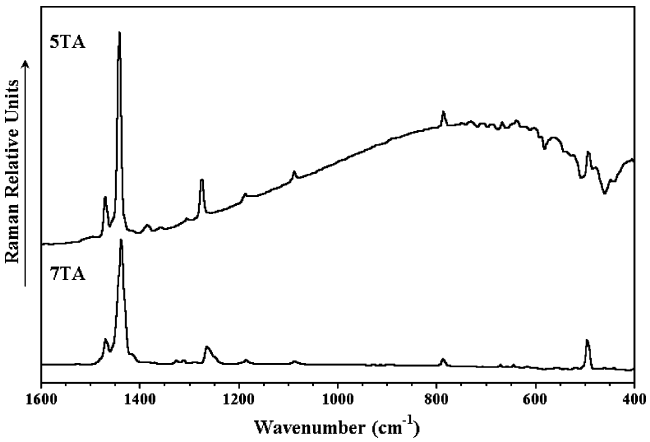

Figure 6. Solid-state FT-Raman spectra of **5TA** and **7TA**. The Nd:YAG laser excitation (λ_{exc}) wavelength was 1064 nm.

this vertical one-electron excitation can be mainly described as the HOMO-1 → LUMO transition. Figure 4 shows that the atomic orbital composition of the HOMO-1 in **5TA** and **7TA** is quite different from that in nonfused α-linked oligothiophenes, being mainly concentrated in the thienoacenes over the innermost fused units and with the greatest contribution now coming from the electron-rich sulfur atoms (i.e., this different topology could justify the closer proximity of the HOMO-1 to the band gap region in the fused oligomers). On the other hand, as mentioned above, the LUMO spreads over the entire frame of π-conjugated C═C/C−C bonds. Consequently, in view of the topologies of the MOs involved in the HOMO-1 → LUMO transition, certain electron density transfer from the sulfur atoms toward the π-conjugated path can be expected to take place upon exciting the absorption band these oligothienoacenes display near 320 nm.

C. Experimental and Theoretical Vibrational Spectra. Figures 5 and 6 display the solid-state FTIR and FT-Raman spectral profiles recorded for **5TA** and **7TA**, respectively, whereas Figure 7 serves to illustrate the selective enhancement of some of the skeletal Raman-active vibrations of **7TA** appearing between 1500 and 1100 cm^{-1}. Finally, Figures 8 and 9 depict the B3LYP/6-31G** vibrational eigenvectors related to the main Raman and IR features, respectively, while Figure 10 shows the dependence with the chain length of the B3LYP/6-31G** Raman spectrum in passing from **5TA** to **7TA**.

From the earliest studies on electrically conducting polymers, vis−NIR electronic absorption and IR and Raman vibrational spectroscopies have been widely used to characterize many

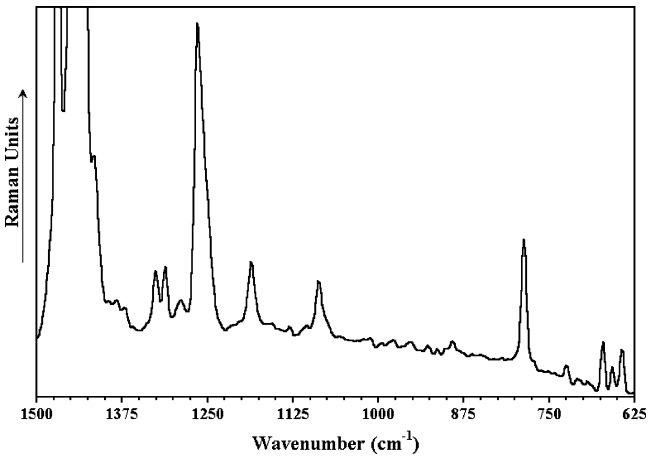

Figure 7. Enlarged profile of the FT-Raman spectrum of **7TA**, recorded on the pure solid, showing the selective enhancement between 1500 and 1100 cm^{-1} of a few scatterings related to specific skeletal stretching modes with respect to the many Raman-active vibrations appearing below 1000 cm^{-1}.

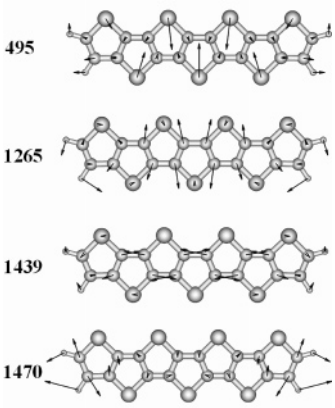

Figure 8. B3LYP/6-31G** vibrational eigenvectors associated with the most outstanding Raman features of **7TA** (experimental frequency values are given in cm^{-1}).

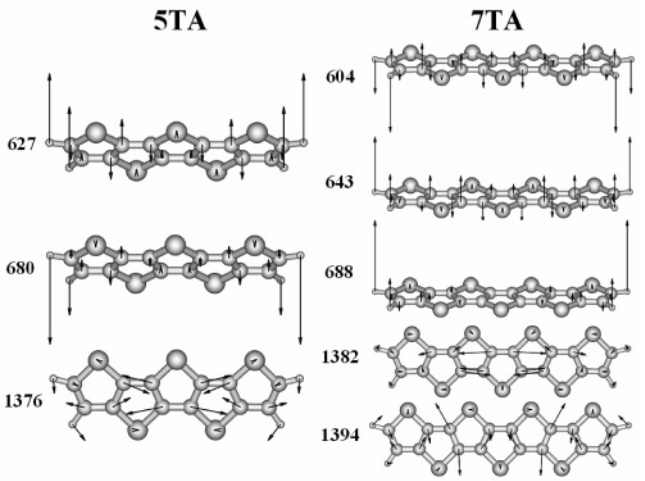

Figure 9. B3LYP/6-31G** vibrational eigenvectors related to some of the strongest IR bands of **5TA** and **7TA** (experimental frequencies are given in cm^{-1}).

different types of π-conjugated systems, both oligomers and polymers, and among them Raman spectroscopy has been shown to be of great help in (i) analyzing the effectiveness of the π-conjugation along a homologous series of oligomers,[19−21] (ii) characterizing different types of conjugational defects induced by either chemical doping or photoexcitation,[22] and (iii) estimat-

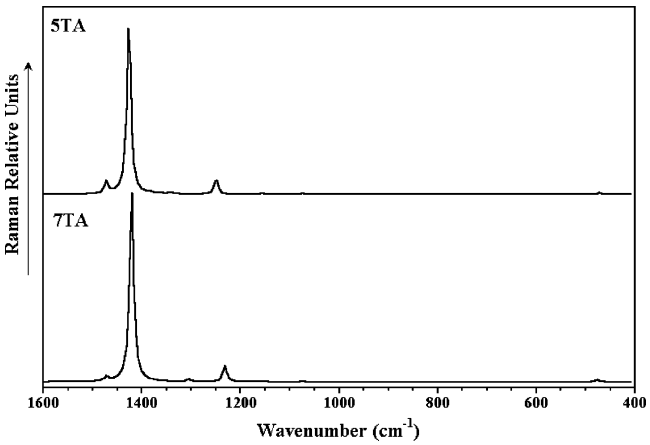

Figure 10. B3LYP/6-31G** Raman spectral profiles computed for **5TA** and **7TA**.

ing the degree of intramolecular charge transfer in push−pull π-conjugated chromophores.[23,24]

The observation of a limited number of overwhelmingly strong Raman scatterings, even for systems having complex chemical structures,[21f,22f] was definitively accounted for over 20 years ago by Zerbi and co-workers through the development of the Effective Conjugation Coordinate (ECC) model. This model, which is now well-accepted, postulates the existence of a unique collective C═C/C−C stretching mode strongly involved in the electron−phonon coupling mechanism which characterizes these one-dimensional π-conjugated chains.[5] In heteroaromatic polyconjugated systems, the so-termed *collective* ECC coordinate has the analytic form of a linear combination of ring C═C/C−C stretchings, which point in the direction from a benzenoid structure (usually that of the ground electronic state) to a quinonoid one (that corresponding to the electronically excited state). The ECC formalism states that the totally symmetric C═C/C−C stretching modes entering in the lattice dynamics of the ECC vibrational coordinate, that is, those which give rise to the few and selectively enhanced Raman features, should undergo large dispersions both in peak position and in intensity upon increasing conjugation length along a given set of neutral oligomers. Thus, changes in Raman frequencies and relative intensities with increasing chain length are particularly useful in evaluating the mean conjugation length for a given family of π-conjugated compounds. Furthermore, upon chemical or electrochemical oxidation/reduction of these π-conjugated heteroaromatic systems, various types of quinonoid-like charged defects are created.[25] The subsequent quinoidization of the π-conjugated backbone gives rise to a further red shift of the strongest Raman lines due to the progressive softening of the conjugated C═C bonds, which is a marker of the type of charged defects created upon oxidation or reduction.[19−22]

Figure 6 shows for these oligothienoacenes the usual simplicity of the Raman profiles commonly found in many types of π-conjugated oligomers, as compared with their rather more complex IR absorption spectra. Thus, while the former displays only three Raman scatterings strongly enhanced with respect to the very many Raman-active vibrations (see Figure 7) at 1470, 1440, and 1265 cm^{-1}, due to ν(C═C) stretchings or in-plane δ(CC) bending modes, the latter shows several features below 1100 cm^{-1}, most of them (i.e., as the strong IR absorptions of **5TA** near 690 and 630 cm^{-1}, due to out-of-plane γ(C−H) bending modes) being fully decoupled from the π-electron degrees of freedom. On the other hand, B3LYP/6-31G** calculations also show that the outstanding IR absorptions recorded at 1393 and 1376 cm^{-1} for **5TA** and 1394 and 1382 cm^{-1} for **7TA** arise from different $\nu(C_\beta-C_\beta)$ stretching modes, for which the motions of the adjacent fused rings take place with opposite phases (see Figure 8), so that these skeletal modes are very weakly coupled with the delocalization of the π-electrons over the whole molecular backbone and consequently they display a vanishing intensity in the Raman spectrum.

TABLE 4: Chain-Length Evolution of the Peak Positions of the Strongest Solid-state Raman Scatterings for the Two Oligothienoacenes under Study (values are given in cm^{-1})

5TA	7TA
1471	1469
1443	1439
1276	1265
1188	1186
1088	1087
789	787
494	495

Table 4 summarizes the evolution of the solid-state Raman peak frequencies upon chain lengthening. The strongest Raman scatterings are those measured near 1470, 1440, and 1270 cm^{-1} (i.e., their selective enhancement among the very many Raman-active vibrations can be observed in the enlarged profiles depicted in Figure 7). The B3LYP/6-31G** vibrational eigenvectors plotted in Figure 9 show that (i) the scattering near 1470 cm^{-1} arises from a totally symmetric ν_{asym}(C═C) stretching mode mainly located on the end fused rings and (ii) whereas that at 1440 cm^{-1} is due to a totally symmetric ν_{sym}(C═C) stretching vibration over the whole frame of fused thienyl rings, along which all the C═C bonds shrink or lengthen in-phase; thus, DFT force field calculations show that these two Raman scatterings are correlated to the characteristic lines A and B, respectively, of the nonfused α-oligothiophenes.[19−21] On the other hand, the Raman peak near 1270 cm^{-1} has no counterpart in common linear α-linked oligothiophenes, being ascribable to a new totally symmetric δ_{sym}(CC) in-plane bending motion mainly located on the inner fused thienyl rings, which gains a noticeable Raman activity upon the replacement of the different β-hydrogens by electron-rich sulfur bridges; namely, in view of its associated eigenvector plotted in Figure 9, it becomes apparent that the structural changes taking place along this collective molecular vibration look like those occurring in the π-conjugated system upon the HOMO → LUMO excitation. Finally, we observe that the Raman scattering measured near 495 cm^{-1} also displays a stronger intensity than in linear α-oligothiophenes; its associated eigenvector shows that it is due again to a totally symmetric δ_{ring} in-plane bending mode with a pronounced collective character, along which all the C−S bonds (i.e., particularly the inner ones) shrink or lengthen in-phase and with similar amplitudes. Its selective enhancement with respect to the huge number of Raman-active vibrations predicted by the optical selection rules suggests that a major role is played by the sulfur atoms in the π-conjugation of these thienoacenes. In this regard, we also would like to highlight that the strong Raman lines A and B are recorded at lower wavenumbers in the oligothienoacenes than in their nonfused counterparts with the same number of double bonds (i.e., lines A and B are recorded at 1530 and 1460 cm^{-1} for **3T** and at 1515 and 1459 cm^{-1} for **4T**, respectively), as a molecular signature of the improved π-conjugation in the former systems due to the higher number of sulfur atoms which likely translates into a softer and more polarizable π-conjugated frame.

The downward dispersion of the strongest Raman scattering from **5TA** to **7TA** (see Table 4) is nicely accounted for by DFT model chemistry, as shown in Figure 10, although the theoretical wavenumbers are lower than the experimental ones, this

mismatch can be ascribed to the well-known tendency of B3LYP/6-31G** data to overestimate π-conjugation. It seems, however, that the peak position of the Raman scattering near 1440 cm^{-1} has not reached saturation for **7TA** but it will continue to red shift with an increasing number of units in the fused planar backbone so that longer oligothienoacenes could still display better π-conjugational properties than **7TA**.

IV. Summary and Conclusions

This work presents an analysis of the molecular scale structural and electronic properties of fused oligothienoacenes having five and seven rings, with potential applications in organic electronics. Their analysis is performed by combining a selection of spectroscopic tools (electromagnetic absorption, fluorescence emission, and FTIR and FT-Raman vibrational spectroscopies), with DFT and TDDFT quantum chemical calculations.

The Raman spectroscopic study of these molecular materials provides analysis within the framework of the ECC theory thus allowing for the dissection of the key Raman features most prominent in overall π-conjugation. Importantly, the collective characters of both the ECC-related vibrational normal modes and the frontier molecular orbital wave functions (i.e., HOMO and LUMO) primarily determine the optical and electronic properties of this class of fused oligothiophenes. In this regard, DFT calculations performed on two linear α-oligothienyl counterparts having the same number of double bonds as the oligothienoacenes show that the bridging of the various β-positions of the α-oligothienyl frame by sulfur linkages stabilizes the HOMO and destabilizes the LUMO, giving rise to a broader energy gap than that of the corresponding nonfused oligothiophene.

These oligothienoacenes, like many other types of π-conjugated oligomers, display a rather simple Raman spectral profile. DFT calculations allowed identification of the vibrations associated with each of the strongest Raman features selectively enhanced by the occurrence of effective π-conjugation. These totally symmetric vibrations are spread over the whole π-conjugated frame indicating their collective character. Furthermore, careful comparison between the FT-Raman spectral profiles of these oligothienocenes and the nonfused α-oligothiophenes has also allowed us to realize the selective intensification for the former class of systems of additional Raman-active vibrational modes, in the low-frequency region, which are also largely involved in the overall π-conjugation. Their precise assignment, on the basis of the molecular dynamics DFT calculations, indicates that they arise from totally symmetric collective vibrations mostly located on the sulfur linkages.

Finally, the downward dispersion of the strongest Raman lines of these oligothienoacenes with respect to their counterparts in nonfused α-linked oligothiophenes is in agreement with an increasing degree of π-conjugation. This spectroscopic result is consistent with the existence in these fused heterocyclic systems of a fully planar and rigid π-conjugated path of unsaturated C_{sp2} atoms, surrounded by several electron-rich and easily polarizable sulfur atoms. In this regard, the comparison between the topologies of the corresponding doubly occupied molecular orbitals higher in energy evidences the significant contribution by the sulfur atoms to MOs that otherwise are of almost pure π-nature in α-oligothiophenes, so that the view of these thienoacenes simply as "rigidified oligothiophenes" may be not adequate at all.

Acknowledgment. Research at the University of Málaga was supported by the Ministerio de Educación y Ciencia (MEC) of Spain through Projects BQU2003-03194 and CTQ2006-14987-C02-01 and by the Junta de Andalucía for funding our FQM-0159 scientific group. R.M.O. is also grateful to MEC and Junta de Andalucía for her personal doctoral grant. Research at the University of Michigan was supported by the National Science Foundation.

References and Notes

(1) Fichou, D. *Handbook of Oligo- and Polythiophenes*; Wiley-VCH: Weinheim, Germany, 1999.

(2) (a) Dodabalapur, A.; Torsi, L.; Katz, H. E. *Science* **1995**, *268*, 270. (b) Garnier, F. *Pure Appl. Chem.* **1996**, *68*, 1455. (c) Horowitz, G.; Deloffre, F.; Garnier, F.; Hajlaoui, R.; Hmyene, M.; Yassar, A. *Synth. Met.* **1993**, *54*, 435.

(3) (a) Mazaki, Y.; Kobayashi, K. *Tetrahedron Lett.* **1989**, *30*, 3315. (b) Sato, N.; Mazaki, Y.; Kobayashi, K.; Kobayashi, T. *J. Chem. Soc., Perkin Trans.* 2 **1992**, *765*.

(4) Zhang, X.; Coté, A. P.; Matzger, A. J. *J. Am. Chem. Soc.* **2005**, *127*, 10502.

(5) (a) Zerbi, G.; Castiglioni, C.; Del Zoppo, M. *Electronic Materials: The Oligomer Approach*; Wiley-VCH: Weinheim, Germany, 1998; p 345. (b) Castiglioni, C.; Gussoni, M.; Lopez Navarrete, J. T.; Zerbi, G. *Solid State Commun.* **1988**, *65*, 625. (c) Lopez Navarrete, J. T.; Zerbi, G. *J. Chem. Phys.* **1991**, *94*, 957 and 965. (d) Hernandez, V.; Castiglioni, C.; Del Zoppo, M.; Zerbi, G. *Phys. Rev. B* **1994**, *50*, 9815. (e) Agosti, E.; Rivola, M.; Hernandez, V.; Del Zoppo, M.; Zerbi, G. *Synth. Met.* **1999**, *100*, 101. (f) Zerbi, G. *Handbook of Conducting Polymers*; Marcel Dekker: New York, 1998.

(6) Frisch, M. J.; Trucks, G. W.; Schlegel, H. B.; Scuseria, G. E.; Robb, M. A.; Cheeseman, J. R.; Montgomery, J. A., Jr.; Vreven, T.; Kudin, K. N.; Burant, J. C.; Millam, J. M.; Iyengar, S. S.; Tomasi, J.; Barone, V.; Mennucci, B.; Cossi, M.; Scalmani, G.; Rega, N.; Petersson, G. A.; Nakatsuji, H.; Hada, M.; Ehara, M.; Toyota, K.; Fukuda, R.; Hasegawa, J.; Ishida, M.; Nakajima, T.; Honda, Y.; Kitao, O.; Nakai, H.; Klene, M.; Li, X.; Knox, J. E.; Hratchian, H. P.; Cross, J. B.; Adamo, C.; Jaramillo, J.; Gomperts, R.; Stratmann, R. E.; Yazyev, O.; Austin, A. J.; Cammi, R.; Pomelli, C.; Ochterski, J. W.; Ayala, P. Y.; Morokuma, K.; Voth, G. A.; Salvador, P.; Dannenberg, J. J.; Zakrzewski, V. G.; Dapprich, S.; Daniels, A. D.; Strain, M. C.; Farkas, O.; Malick, D. K.; Rabuck, A. D.; Raghavachari, K.; Foresman, J. B.; Ortiz, J. V.; Cui, Q.; Baboul, A. G.; Clifford, S.; Cioslowski, J.; Stefanov, B. B.; Liu, G.; Liashenko, A.; Piskorz, P.; Komaromi, I.; Martin, R. L.; Fox, D. J.; Keith, T.; Al-Laham, M. A.; Peng, C. Y.; Nanayakkara, A.; Challacombe, M.; Gill, P. M. W.; Johnson, B.; Chen, W.; Wong, M. W.; Gonzalez, C.; Pople, J. A. *Gaussian* 03, revision B.04; Gaussian Inc.: Pittsburgh, PA, 2003.

(7) Becke, A. D. *J. Chem. Phys.* **1993**, *98*, 1372.

(8) Stephens, P. J.; Devlin, F. J.; Chabalowski, F. C. F.; Frisch, M. J. *J. Phys. Chem.* **1994**, *98*, 11623.

(9) Novoa, J. J.; Sosa, C. *J. Phys. Chem.* **1995**, *99*, 15837.

(10) Scott, A. P.; Radom, L. *J. Phys. Chem.* **1996**, *100*, 16502.

(11) Rauhut, G.; Pulay, P. *J. Phys. Chem.* **1995**, *99*, 3093.

(12) Francl, M. M.; Pietro, W. J.; Hehre, W. J.; Binkley, J. S.; Gordon, M. S.; Defrees, D. J.; Pople, J. A. *J. Chem. Phys.* **1982**, *77*, 3654.

(13) Runge, E.; Gross, E. K. U. *Phys. Rev. Lett.* **1984**, *52*, 997. Gross, E. K. U.; Kohn, W. *Adv. Quantum Chem.* **1990**, *21*, 255. *Density Functional Theory*; Gross, E. K. U., Driezler, R. M., Eds.; Plenum Press: New York, 1995; p 149.

(14) Casida, M. E. *Recent Advances in Density Functional Methods, Part I*; Chong, D. P., Ed.; World Scientific: Singapore, 1995; p 115.

(15) Koch, W.; Holthausen, M. C. *A Chemist's Guide to Density Functional Theory*; Wiley-VCH: Weinheim, Germany, 2000.

(16) Casado, J.; Miller, L. L.; Mann, K. R.; Pappenfus, T. M.; Kanemitsu, Y.; Ortí, E.; Viruela, P. M.; Pou-Amérigo, R.; Hernandez, V.; López Navarrete, J. T. *J. Phys. Chem. B* **2002**, *106*, 3872.

(17) Portmann, S.; Lüthi, H. P. *Chimia* **2000**, *54*, 766−770.

(18) Zhang, X.; Matzger, A. J. *J. Org. Chem.* **2003**, *68*, 9813.

(19) Sakamoto, A.; Furukawa, Y.; Tasumi, M. *J. Phys. Chem.* **1994**, *98*, 4635.

(20) (a) Yokonuma, N.; Furukawa, Y.; Tasumi, M.; Kuroda, M.; Nakayama, J. *Chem. Phys. Lett.* **1996**, *255*, 431. (b) Harada, I.; Furukawa, Y. *Vibrational Spectra and Structure*; Durig, J., Ed.; Elsevier: Amsterdam, The Netherlands, 1991; Vol. 19, p 369.

(21) (a) Hernandez, V.; Casado, J.; Ramirez, F. J.; Zotti, G.; Hotta, S.; Lopez Navarrete, J. T. *J. Chem. Phys.* **1996**, *104*, 9271. (b) Casado, J.; Hernandez, V.; Hotta, S.; Lopez Navarrete, J. T. *J. Chem. Phys.* **1998**, *109*, 10419. (c) Moreno Castro, C.; Ruiz Delgado, M. C.; Hernandez, V.; Hotta, S.; Casado, J.; Lopez Navarrete, J. T. *J. Chem. Phys.* **2002**, *116*, 10419. (d) Moreno Castro, C.; Ruiz Delgado, M. C.; Hernandez, V.; Shirota, Y.; Casado, J.; Lopez Navarrete, J. T. *J. Phys. Chem. B* **2002**, *106*, 7163. (e) Ruiz Delgado, M. C.; Hernandez, V.; Lopez Navarrete, J. T.; Tanaka, S.;

Yamashita, Y. *J. Phys. Chem. B* **2004**, *108*, 2516. (f) Ruiz Delgado, M. C.; Casado, J.; Hernandez, V.; Lopez Navarrete, J. T.; Fuhrmann, G.; Bauerle, P. *J. Phys. Chem. B* **2004**, *108*, 3158. (g) Casado, J.; Ponce Ortiz, R.; Ruiz Delgado, M. C.; Azumi, R.; Oakley, R. T.; Hernandez, V.; Lopez Navarrete, J. T. *J. Phys. Chem. B* **2005**, *109*, 10115.

(22) (a) Casado, J.; Hernandez, V.; Hotta, S.; Lopez Navarrete, J. T. *J. Chem. Phys.* **1998**, *109*, 10419. (b) Casado, J.; Hernandez, V.; Hotta, S.; Lopez Navarrete, J. T. *Adv. Mater.* **1998**, *10*, 1258. (c) Casado, J.; Miller, L. L.; Mann, K. R.; Pappenfus, T. M.; Kanemitsu, Y.; Orti, E.; Viruela, P. M.; Pou-Amerigo, P.; Hernandez, V.; Lopez Navarrete, J. T. *J. Phys. Chem. B* **2002**, *106*, 3872. (d) Casado, J.; Miller, L. L.; Mann, K. R.; Pappenfus, T. M.; Hernandez, V.; Lopez Navarrete, J. T. *J. Phys. Chem. B* **2002**, *106*, 3597. (e) Casado, J.; Ruiz Delgado, M. C.; Shirota, Y.; Hernandez, V.; Lopez Navarrete, J. T. *J. Phys. Chem. B* **2003**, *107*, 2637. (f) Casado, J.; Hernandez, V.; Ponce Ortiz, R.; Ruiz Delgado, M. C.; Lopez Navarrete, J. T.; Fuhrmann, G.; Bauerle, P. *J. Raman Spectrosc.* **2004**, *35*, 592.

(23) (a) Hernandez, V.; Casado, J.; Effenberger, F.; Lopez Navarrete, J. T. *J. Chem. Phys.* **2000**, *112*, 5105. (b) Delgado Ledesma, S.; Ponce Ortiz, R.; Ruiz Delgado, M. C.; Vida, Y.; Perez-Inestrosa, E.; Casado, J.; Hernandez, V.; Kim, O.-K.; Lehn, J.-M.; Lopez Navarrete, J. T. *Chem.—Eur. J.* **2004**, *10*, 3805.

(24) (a) Gonzalez, M.; Segura, J. L.; Seoane, C.; Martin, N.; Garin, J.; Orduna, J.; Alcala, R.; Villacampa, B.; Hernandez, V.; Lopez Navarrete, J. T. *J. Org. Chem.* **2001**, *66*, 8872. (b) Casado, J.; Pappenfus, T. M.; Miller, L. L.; Mann, K. R.; Orti, E.; Viruela, P. M.; Pou-Amerigo, P.; Hernandez, V.; Lopez Navarrete, J. T. *J. Am. Chem. Soc.* **2003**, *125*, 2534.

(25) (a) Ehrendorfer, Ch.; Karpfen, A. *J. Phys. Chem.* **1994**, *98*, 7492. (b) Ehrendorfer, Ch.; Karpfen, A. *J. Phys. Chem.* **1995**, *99*, 5341.